Determination of the Synthesis Diagram of Sodium Cobalt Oxide and Electrochemical Study

by

YUECHUAN LEI

B.S. Materials Science and Engineering
Tsinghua University (2012)

Submitted to the Department of Materials Science and Engineering
in Partial Fulfillment of the Requirements for the Degree of

MASTER OF SCIENCE

at the

MASSACHUSETTS INSTITUTE OF TECHNOLOGY

June 2014

Signature redacted

Signature of Author .....
Department of Materials Science and Engineering
May 22, 2014

Signature redacted

Certified by .....
Gerbrand Ceder
R. P. Simmons Professor of Materials Science and Engineering
Thesis Supervisor

Signature redacted

Accepted by .....
Gerbrand Ceder
R. P. Simmons Professor of Materials Science and Engineering
Chair, Departmental Committee on Graduate Students

Determination of the Synthesis Diagram of Sodium Cobalt Oxide and Electrochemical Study

by

Yuechuan Lei

Submitted to the Department of Materials Science and Engineering
on May 23, 2014 in Partial Fulfillment of the Requirements for the Degree of
Master of Science in Emerging, Fundamental, and Computational Studies in Materials

Abstract

A complete and uniform synthesis diagram of Na_xCoO_2 has been proposed based on forty-one samples synthesized at various temperatures from 450°C to 750°C by solid-state reactions with initial Na:Co ratio ranging from 0.60 to 1.05. Four monophasic domains of O3, O3', P3' and P2 and four biphasic regions were revealed based on an XRD analysis. The sodium contents in these phases were determined according to the d_{00l}-x relations obtained by an *in situ* XRD experiment and it is found O3, O3' and P3' phase almost form with only one stoichiometry, that is x=1.00, 0.83 and 0.67 respectively, by solid-state reaction while P2 phase forms in a slightly larger composition range from 0.68 to 0.76. Galvanostatic charging on O3-$Na_{1.00}CoO_2$ battery reveals several plateaus and steep steps on the voltage curve, the corresponding phase transitions and solid solution behaviors were studied by a simultaneous *in situ* XRD experiment. The composition driven structural evolution in three layer Na_xCoO_2 follows the sequence: O3-O3'-P3'-P3-P3', with a generally increased interslab distance d_{00l}.

Thesis Supervisor: Gerbrand Ceder
Title: R.P. Simmons Professor of Materials Science and Engineering

Acknowledgement

Above all, I would like to express my greatest gratitude and special thanks to my thesis advisor, Professor Gerbrand Ceder, for his thoughtful guidance and tremendous encouragement that allows me to complete this work. Through his insightful understanding in both theoretical and experimental perspective of the materials science, Prof. Ceder has enlightened me and broadened my horizons in the field of sodium ion battery. His passion and foresight for the development of novel energy storage materials made my research more fruitful and productive.

I would also like to express my very special appreciation to Xin Li and Lei Liu who has generously shared their experimental skills, research understanding and insights with me. They literally helped and guided me through my darkest days at MIT. I feel extremely lucky to have them as my colleagues, mentors as well as friends, with whom I could share not only my research progress, but also my joys and sorrows. It was a great pleasure to work and interact with other members in our experimental team, Dr. Xiaohua Ma, Prof. Hailong Chen, Nancy Twu, Dr. Jae Chul Kim, Jinhyuk Lee, Di Wu, Rui Wang, Dr. Plousia Vassilaras and Ian Matts. I really appreciated the time they spent sharing their experiences and skills with me so that I could adapt to this lab and make progress in my research without too much detouring. It was more than a comfortable experience to collaborate closely with them.

I would thank all other theoretical team members and alumni in the Ceder group as well. Prof. Yifei Mo, Dr. Yabi Wu, Dr. Rahul Malik, Dr. Ruoshi Sun, Prof. Shyue Ping Ong, Dr. Pieremanuele Canepa, Dr. Sai Jayaraman, Dr. Alexander Urban, Dr. Dong-Hwa Seo, Dr. Eric Wang, Dr. Bo Xu, Dr. Hong Zhu, Aziz Abdellahi, Stephen Dacek, Wenxuan Huang, Daniil Kitchaev, William Richards, Ziqin Rong, Wenhao Sun, Alexandra Toumar, Lusann Wren Yang, Sai Gautam, ShinYoung Kang and Kathryn E. Simons have provided me with a very friendly but stimulating environment and atmosphere for research. I was so lucky to have discussions, idea exchanges and casual chats with these nice and brilliant people.

At last I would say I could not thank my parents more than enough for their unconditional love and unlimited support under all circumstances, which I shall never forget as long as I live. I am really grateful that they respect and support all my major decisions in my life, instead of expressing their doubt, which allows me to become who I am today. Without their encouragement, this work would never be accomplished and I would never made it today.

Table of Contents

List of Figure Captions

List of Table Captions

CHAPTER 1

MOTIVATION AND BACKGROUND

OVERVIEW OF THE THESIS

1.1 Motivation and Background

1.1.1 Category of Layered Na-ion Battery Cathode Materials and Performance

Na_xMO_2 or $Na_xM_{(1)}M_{(2)...}O_2$ (M=transition metal) have been widely studied as cathode materials in Sodium Ion Batteries. These layered electrode materials can be generally categorized into two major groups, P2 type and O3 type, according to Delmas' notation[1]. Both types can exhibit decently good repeatable reversible capacity[2,3]. Their structural variations during electrochemical intercalation or deintercalation of Na ions, however, are very distinct. The P2 type compounds usually retain the P2 framework, while various Na vacancy orderings and superstructures form, upon charging or discharging[4–8]. Though not common, P2-O2[9,10] and P2-OP4[3] transitions have also been observed in the high voltage range. In contrast to P2, the O3 type compounds usually experience more severe structure changes during Na deintercalation in the lower voltage range. O3-O3'-P3/P3' phase transitions have been confirmed by in situ or ex situ XRD studies in various systems[11–16]. Thus, to understand the phase stability of Na_xMO_2 (or $Na_xM_{(1)}M_{(2)...}O_2$) and the thermodynamics behind are becoming an increasingly important task. Among many layered Na_xMO_2 compounds, Na_xCoO_2 system had been studied as cathode materials since 1980s[11,17]. The discovery of large thermoelectric power in $Na_{0.5}CoO_2$ single crystal[18], and of superconductivity in P2-$Na_{0.35}CoO_2 \cdot 1.3H_2O$[19] made Na_xCoO_2 an active area of study. Sodium cobalt oxide, therefore, becomes an

appropriate candidate material as a prototype system for our study on its phase stability.

1.1.2 Development Background of Sodium Cobalt Oxide

The earliest Na_xCoO_2 phase diagram proposed in 1973[20] had shown that four different phases of Na_xCoO_2 could be synthesized by classic solid-state reaction, known as α(also O3), α'(also O3' or O1), β(also P3' or P1) and γ(also P2). All these phases have layer structures containing sheets of CoO_6 octahedra with Na^+ ions intercalated between them. Following the notation of Delmas[1], the O or P designation refers to structure in which Na^+ is octahedrally or prismatically coordinated by oxygen, while the numerical designations refer to the repeat period of the transition metal stacking. The prime mark, however, indicates the structure may have experienced a monoclinical distortion from its parent structure[11]. Na_xCoO_2 with various x can be obtained by conventional solid-state reaction, chemical and electrochemical intercalation or deintercalation of sodium ions[11,21–23]. Previous reports on synthesis of Na_xCoO_2 based on solid-state reaction have been summarized in Table 1. The P2 phase could usually be obtained at higher temperature (650°C-900°C) when $0.55<x<0.88$, while the three layer structures, O3, O3' and P3', were synthesized when $0.92<x<1.00$, $0.75<x<0.83$ and $0.60<x<0.67$ respectively in the lower T range (500°C-550°C). Though many intensive studies on Na_xCoO_2 system have been carried out before, including an in situ study on the P2 phase[4] and an ex situ study on the three layer structures[11], a uniform synthesis

diagram and an in situ study on the three layer compounds are still absent, which may provide us with more information in details.

Table 1. The compositions and structure types of Na_xCoO_2 and the corresponding synthesis conditions by solid-state reaction. Ref. 24 indicates that the sodium content x given may be nominal values. If there are two values of interslab distance for one compound, it indicates two phases were observed in the experiment from the original references.

Compound	Structure type	Synthesis temperature	Interslab distance	Compound	Structure type	Synthesis temperature	Interslab distance
$Na_{0.88}CoO_2$[24]	P2	900°C	5.4310 or 5.4040	$Na_{0.92}CoO_2$[21]	O3	550°C	5.1999
$Na_{0.77}CoO_2$[24]	P2	900°C	5.4475 or 5.4435	$Na_{0.83}CoO_2$[17]	O3′	550°C	-
$Na_{0.75}CoO_2$[23]	P2	800°C	-	$Na_{0.75}CoO_2$[21]	O3′	550°C	5.3670
$Na_{0.75}CoO_2$[22]	P2	800°C	5.4072 or 5.4378	$Na_{0.75}CoO_2$[20]	O3′	500°C	5.3766
$Na_{0.74}CoO_2$[4]	P2	850°C	-	$Na_{0.67}CoO_2$[17]	P3′	550°C	-
$Na_{0.72}CoO_2$[20]	P2	>650°C	5.4500	$Na_{0.67}CoO_2$[26]	P3′	530°C	5.4992
$Na_{0.67}CoO_2$[17]	P2	750°C	-	$Na_{0.62}CoO_2$[27]	P3′	550°C	5.4923
$Na_{0.66}CoO_2$[24]	P2	900°C	5.4585	$Na_{0.62}CoO_2$[24]	P3′	550°C	5.4922
$Na_{0.55}CoO_2$[24]	P2	900°C	5.4735	$Na_{0.60}CoO_2$[21]	P3′	550°C	5.4871
$Na_{1.00}CoO_2$[20]	O3	500°C	5.1900	$Na_{0.60}CoO_2$[20]	P3′	500°C	5.5100
$Na_{1.00}CoO_2$[25]	O3 (single crystal)	1050-850°C	5.2030				

1.2 Overview of the Thesis

In this work, we report a complete and uniform synthesis diagram of Na_xCoO_2, obtained by classic solid-state reaction. A detailed structural study was carried out using X-Ray powder diffraction and the sodium compositions in layer structure were determined by the structure refinements which are compared with calculations based on an in situ XRD study. Our results show, in contrast to previous reports, most phases are layer compounds forming with a single sodium stoichiometry, and the actual sodium content in the layer structure can deviate significantly from nominal composition. For clarity, we define $\phi_{Na:Co}$ as the initial Na:Co ratio or nominal sodium content in this paper, while x in Na_xCoO_2 stands for actual sodium composition. It is found that pure O3 phase, previously reported to exist in the range of $0.90<x<1.00$, can only exist as $Na_{1.00}CoO_2$ below 450°C; And O3' phase, which has a monoclinically distorted single layer structure, can only form $Na_{0.83}CoO_2$ by solid-state reaction, even though $\phi_{Na:Co}$ ranges from 0.68 to 1.00; Similarly, P3' phase, which also has a weak monoclinically distorted single layer structure with Na ions in prismatic sites, forms with a single stoichiometry around $Na_{0.67}CoO_2$ by solid-state reaction between 500-550°C; Pure P2 phase, however, forms in a relatively larger range of $0.68<x<0.76$ above 750°C. We also found that, for the first time, by electrochemical deintercalation, P3 phase without monoclinical distortion can be obtained near $x=0.56$ ($\approx 5/9$) under room temperature.

CHAPTER 2

EXPERIMENTAL METHODS

2.1 Synthesis and Characterization

2.1.1 Synthesis by Solid-State Reaction

Samples of Na_xCoO_2 with $0.60<\phi_{Na:Co}<1.05$ were synthesized by solid state reaction at different temperatures ranging from 450°C to 750°C. Stoichiometric amounts of Na_2O_2 (Alfa, 95%) and Co_3O_4 (Alfa, 99.7%) powders were mixed and thoroughly ground by high-energy ball milling before pressing into pellets. Samples were treated carefully to minimize air contact till they were placed in a box furnace. The temperature was slowly (5°C/min) increased to certain values within 450°C-750°C, held constant for 16h in air. And the samples were then quenched to room temperature and quickly moved to an Ar-filled glove box. Forty-one samples in total, except for four O3 samples that were synthesized at 450°C in a tube furnace with O_2 flow, were synthesized using this method in order to give a full picture of synthesis diagram.

2.1.2 Structural Characterization by XRD

All samples were analyzed by X-Ray powder diffraction on a Rigaku Rotaflex or PANalytical X' Pert pro diffractometer equipped with Cu Kα radiation. Data were collected in the 2θ range of 10°-85° at a scan rate of 0.021° s^{-1} or slower. All the samples were well sealed using Kapton film to avoid air contact or moisture contamination. The structural information and lattice parameters were determined using Rietveld refinement, as described in detail later. Sodium contents of Na_xCoO_2

for all samples in the single-phase region were determined by a comparison with in situ XRD results, as described in detail later.

2.2 Electrochemical Deintercalation of Sodium

Electrochemical studies and a simultaneous in situ XRD experiments are carried out on Na/1M $NaPF_6$ in EC:DEC/O3-$Na_{1.00}CoO_2$ batteries, which is specially designed that enables XRD signals to be collected through a Be window. The positive electrodes consist of 80 wt% of active material, 15 wt% of carbon black and 5 wt% of PTFE as a binder. And a glass fiber filter was used as a separator. The airtight cells were carefully assembled inside an Ar-filled glove box to avoid any air or moisture contact with Sodium metal anode and O3-$Na_{1.00}CoO_2$ cathode. The battery was charged from 2.5v to 3.4v (corresponding to $1.00>x>0.52$) at a rate of C/50 (4.8 mA g^{-1}) at room temperature. The simultaneous in situ XRD experiments were performed in a repeated manner on a Bruker D8 X-Ray diffractometer equipped with a Mo source ($\lambda_{K\alpha 1} = 0.7093\ \dot{A}$). Each scan was carried out at a scan speed of 0.0065° s^{-1} in the whole 2θ range, from 6.5° to 30°, to give full XRD patterns in detail. This setup and configuration generates a complete scan every one hour with Na composition resolution Δx=0.02.

CHAPTER 3

RESULTS AND ANALYSIS

3.1 The Construction of a Synthesis Diagram of Sodium Cobalt Oxide

3.1.1 An Overview

A total number of forty-one effective samples were synthesized in the selected range of interest (450°C<T<750°C, $0.60<\phi_{Na:Co}<1.05$), nineteen of which fall into single phase regions without forming other layer structure, while the other twenty-two samples contain more than one kind of layered compounds. These results were given according to phase identifications based on X-ray powder diffraction. All four known phases (O3, O3', P3', P2) of Na_xCoO_2 have been successfully synthesized in the selected range in this study, and four single-phase regions of them have been identified based on experimental data points. These results have been reorganized and plotted to give a complete and uniform experimental synthesis diagram (Fig. 2). The O3 and P2 phases, which have been previously studied extensively, can be synthesized at lower temperature with higher $\phi_{Na:Co}$ and at higher temperature with lower $\phi_{Na:Co}$ respectively as expected. The P3' phase can be obtained in a narrow temperature window around 550°C when sodium is highly deficient and this result is generally consistent with earlier reports. The O3' phase, however, can be synthesized over an unexpected large initial Na:Co ratio range, from $\phi_{Na:Co}$=0.68 (or even lower) to $\phi_{Na:Co}$=1.00, forming a narrow diagonal band on the synthesis diagram. Corresponding two-phase regions can be identified between any two single-phase regions.

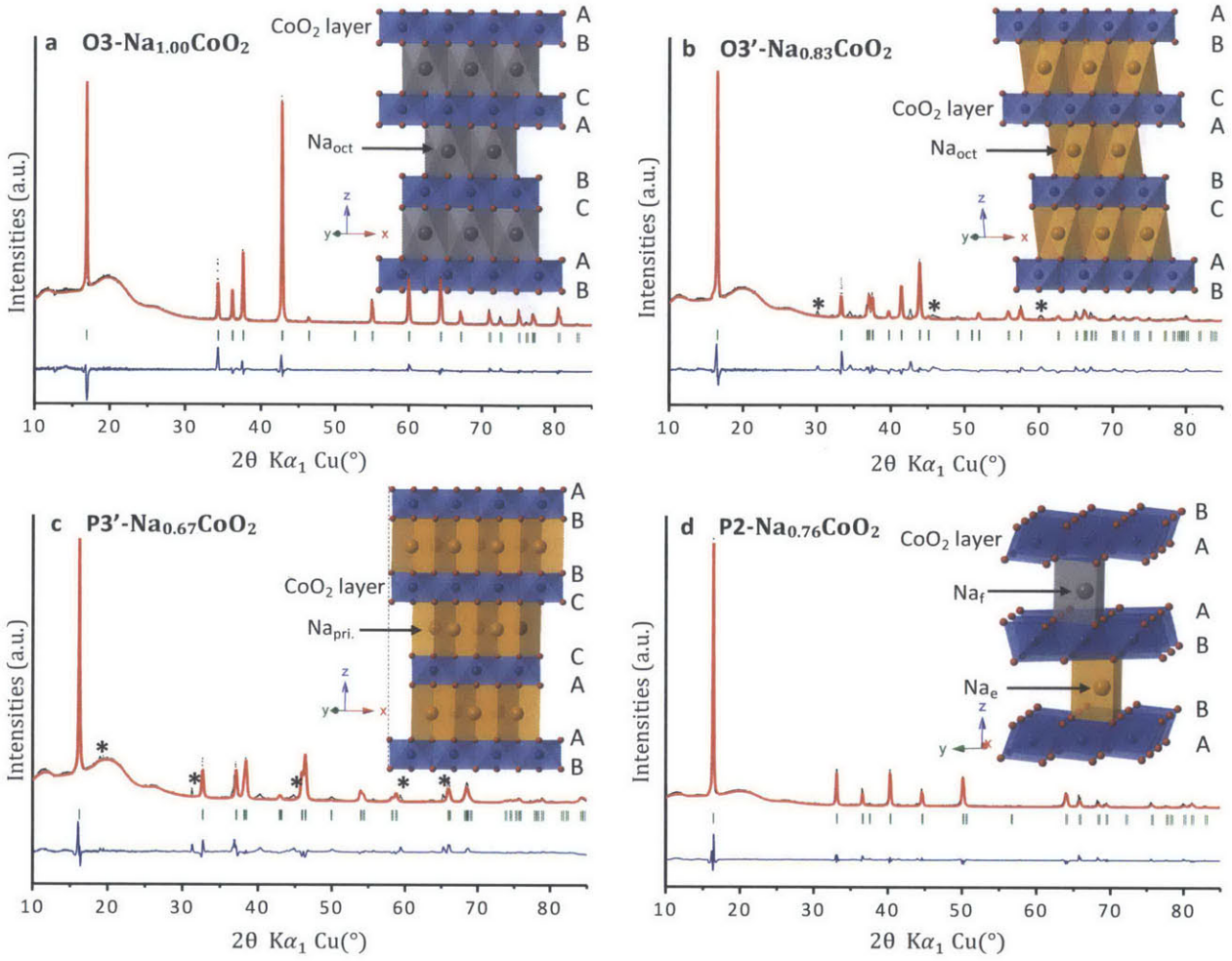

Figure 1 | Structural characterization of four different phases of Na_xCoO2. Observed (black dots) and calculated (red lines) XRD patterns for O3-$Na_{1.00}CoO_2$ (R_{wp}=14.3%) with $\phi_{Na:Co}$=1.05 and T=450℃ (a), O3'-$Na_{0.83}CoO_2$ (R_{wp}=19.8%) with $\phi_{Na:Co}$=1.00 and T=650℃ (b), P3'-$Na_{0.67}CoO_2$ (R_{wp}=19.0%) with $\phi_{Na:Co}$=0.68 and T=535℃ (c), P2-$Na_{0.76}CoO_2$ (R_{wp}=15.2%) with $\phi_{Na:Co}$=0.76 and T=750℃ (d) were given based on Rietveld refinements. The broad peaks between 10° and 30° are due to the Kapton film used to seal the samples. The residual discrepancy (blue lines) and peak positions (green bars) are also given beneath each pattern. Peaks marked by * in (b) are due to Na ions ordering and superstructures[20] in the O3' structure, while Peaks with * mark in (c) are impurities of Co_3O_4 precursor. The additional structural information in detail can be found in Table 2. Symbols A, B and C in the schematics (insets) represent layers of oxygen with different stacking. In the O3 and O3' structures, all Na ions reside in edge sharing octahedral sites while in the P3' structure, Na ions have prismatic coordination with one side edge sharing and another face sharing. There are, however, two kinds of prismatic sites for Na ions in the P2 structure, they are edge sharing and face sharing sites.

3.1.2 Structural Characterization

A detailed structural investigation on each phase was performed by XRD analysis using the Rietveld method. The structural information and synthesis conditions of representative samples of each phase were given in Table 2. The O3 phase sample $Na_{1.00}CoO_2$ ($\phi_{Na:Co}$=1.05, T=450°C) has an XRD pattern that could be indexed within the trigonal space group $R\bar{3}m$ (No.166), while the O3' phase sample $Na_{0.83}CoO_2$ ($\phi_{Na:Co}$=1.00, T=650°C) and the P3' phase sample $Na_{0.67}CoO_2$ ($\phi_{Na:Co}$=0.68, T=535°C) were indexed based on monoclinic cells in the space group $C2/m$ (No.12). Both of the P2 phase samples $Na_{0.68}CoO_2$ ($\phi_{Na:Co}$=0.68, T=750°C) and $Na_{0.76}CoO_2$ ($\phi_{Na:Co}$=0.76, T=750°C) could be well indexed with a hexagonal cell in the space group $P6_3/mmc$ (No.194). Observed and calculated XRD patterns of all four

Table 2. The cell parameters and synthesis conditions of representative samples for each phase of Na_xCoO_2

Compound	Space group	Cell constants (A)	volume (A^3)	Volume/f.u. (A^3)	Structure type	Synthesis conditions
$Na_{1.00}CoO_2$	$R\bar{3}m$ (No.166)	$a = 2.8883$ $c = 15.6019$	112.718	37.573	O3	$\phi_{Na:Co}$=1.05 T=450°C
$Na_{0.83}CoO_2$	$C2/m$ (No.12)	$a = 4.8912$ $b = 2.8681$ $c = 5.7937$ $\beta = 111.84°$	75.443	37.722	O3'	$\phi_{Na:Co}$=1.00 T=650°C
$Na_{0.67}CoO_2$	$C2/m$ (No.12)	$a = 4.9126$ $b = 2.8270$ $c = 5.7087$ $\beta = 106.06°$	76.188	38.094	P3'	$\phi_{Na:Co}$=0.68 T=535°C
$Na_{0.68}CoO_2$	$P6_3/mmc$ (No.194)	$a = 2.8320$ $c = 10.8971$	75.690	37.845	P2	$\phi_{Na:Co}$=0.68 T=750°C
$Na_{0.76}CoO_2$	$P6_3/mmc$ (No.194)	$a = 2.8381$ $c = 10.8265$	75.522	37.761	P2	$\phi_{Na:Co}$=0.76 T=750°C
$Na_{0.56}CoO_2$	$R3m$ (No.160)	$a = 2.8192$ $c = 16.5880$	114.176	38.059	P3	Electrochemical deintercalation of Na from O3-$Na_{1.00}CoO_2$

phases were compared and given in Fig. 1, these results confirmed the purity of each sample. Other samples in the same single-phase regions, whose structural information is not presented here, are isostructural with the representative sample of each phase, while the lattice parameters can be slightly different.

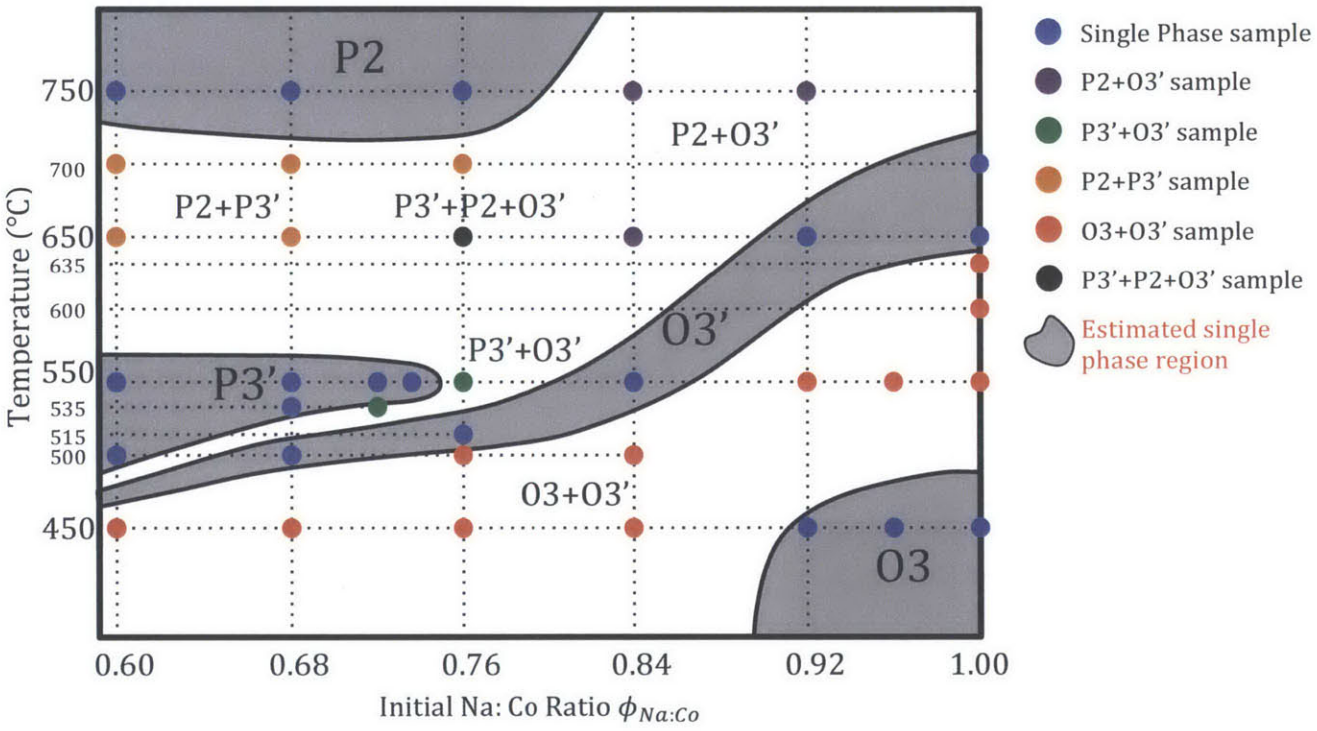

Figure 2 | Synthesis diagram of Na_xCoO_2 as a function of the initial Na:Co ratio $\phi_{Na:Co}$ (X axis) and the sintering temperature (Y axis). A total number of 41 samples, including 19 samples (only 18 are shown, the one with $\phi_{Na:Co}$=1.05 and T=450° falls out of this diagram) containing only one layered structure (filled blue circles) and 22 samples containing more than one identified layered compounds (filled circles in other colors), had been synthesized to determine the synthesis diagram. The single-phase regions (grey areas) and the biphasic domains (white areas) were estimated based on experimental data points shown. In order to rule out all other potential factors that may influence the results, all other conditions of synthesis, except T and $\phi_{Na:Co}$, have been set constant. Since the x in Na_xCoO_2 can deviate significantly from initial Na:Co ratio, $\phi_{Na:Co}$ is used in this diagram instead of x. In addition, those samples being in the nominal single-phase regions indicates they were not contaminated by other layered structures, however, some of these samples also contain small amount of Co_3O_4 impurities. Most samples that fall into biphasic domains contain certain amount of Co_3O_4 precursor, which is not reflected in this synthesis diagram.

3.2 Electrochemistry of Three Layer Type

3.2.1 Motivation and Target

In order to obtain the d_{00l}-x relation that enables us to determine actual sodium content in layer structure obtained by solid-state reaction, an electrochemical study and a simultaneous in situ XRD experiments are carried out. A synergy between electrochemistry and in situ XRD through sodium ion deintercalation (first charge) in three layered series was plotted, as shown in Fig. 3. As a consequence of preferred orientation of the active material in the cathode during electrode preparation, all c related ($00l$) peaks are enhanced while all other a or b related peaks are suppressed. It becomes, therefore, not practical to retrieve precise information on the a or b parameters from in situ XRD patterns. Since ($00l$) peaks have very strong signals, we can clearly identify O3, O3' and P3' monophasic regions, observe O3-O3', O3'-P3' phase transitions and accurately calculate d_{00l} or c based on ($00l$) peak positions.

3.2.2 Phase Variations during Na Deintercalation

Based on a direct comparison between the in situ XRD patterns and the voltage curve during charge, as shown in Fig. 3, the first step at x=1.00 and the second step between 0.81 and 0.88 on the voltage curve corresponds to O3 and O3' single phase domain and the steep step at x=0.67 marks the start of P3' monophasic region. The two plateaus between these steps characterize the biphasic domains of O3+O3' and O3'+P3'. A continuous increase of voltage at lower x range (smaller

than 0.67) characterizes the P3' single phase existing over a wide composition range.

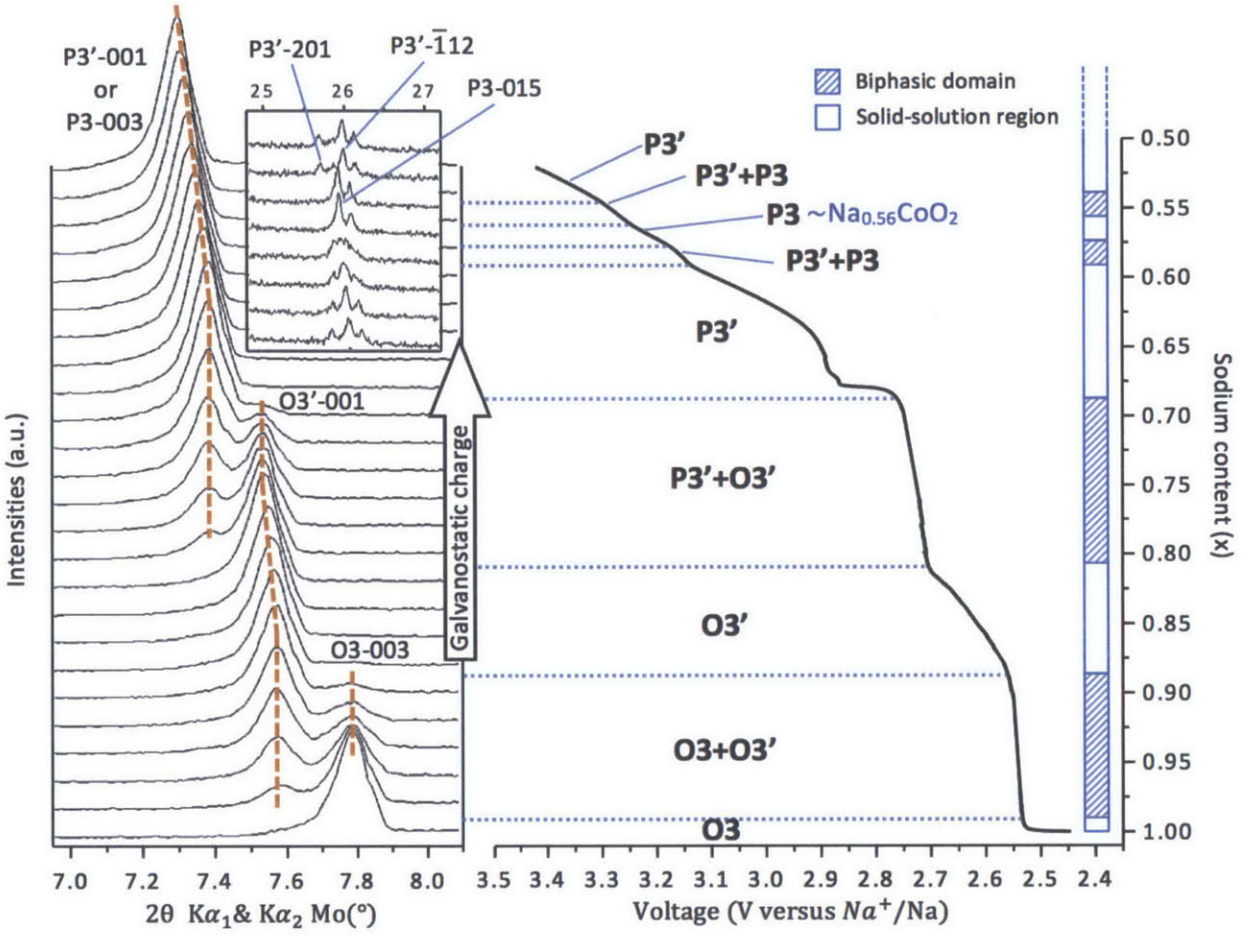

Figure 3 | Synergy between electrochemistry and in situ XRD through sodium ion deintercalation in three-layer Na_xCoO_2 starting from O3-$Na_{1.00}CoO_2$. The galvanostatic electrochemical battery charge (right side) enables us to obtain a continuously decreasing x while in situ XRD scans can be carried out simultaneously in a repeated manner. Each XRD scan takes 1 hour which corresponds to Δx=0.02. The resulting in situ XRD experiment (left side) shows clearly either solid-solution behaviors in the single-phase regions, characterized by a peak shifting, or phase transitions between two phases, characterized by the coexistence of two distinct 00l peaks. The shifting or transition of 00l peaks to lower 2θ positions (red dashed lines) is consistent with the interslab distance increase during sodium deintercalation. The combination of 201 and $\bar{1}$12 peaks and the successive splitting of 015 peak (top left inset) characterize the P3'-P3-P3' phase transition. The correlation between the in situ XRD patterns and the electrochemical behaviors enables us to calculate the interslab distance in each phase as a function of x.

Another two small plateaus and one step between them, however, were found near x=0.56. A closer examination of the XRD profiles at around 2θ =26° reveals a P3'-P3-P3' phase transition in a very narrow composition range. The P3'-201 peak and P3'-$\bar{1}$12 peak joined at x=0.56 and the P3-015 peak split again afterwards, as shown in Fig 4 top left inset. The additional peaks nearby are due to Mo $K\alpha 2$ radiation. In order to clearly analyze the P3-$Na_{0.56}CoO_2$, an *ex situ* XRD test has been carried out on the same sample as shown in Fig. 4. By comparing the XRD profile of P3 (Fig. 4

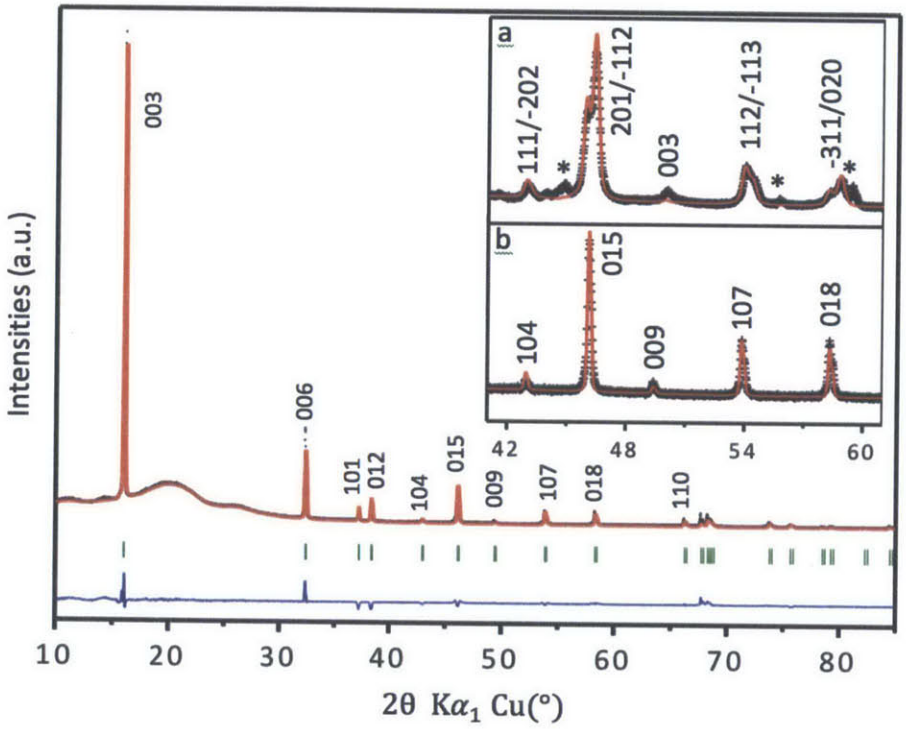

Figure 4 | Ex situ XRD characterization of P3-$Na_{0.56}CoO_2$. Observed (black dots) and calculated (red lines) XRD profiles for P3-$Na_{0.56}CoO_2$ were given. A Rietveld refinement was carried out in space group R3m (No. 160), which gives a=2.8192 $\dot{A}$, c=16.5880 $\dot{A}$, R_{wp}=15.08%. The residual discrepancy (blue lines) and peak positions (green bars) are also given beneath the pattern. Observed (crosses) and calculated (red lines) XRD patterns of P3' (inset a) and P3 (inset b) in the range of 41°<2θ<61° were compared in detail. Peaks marked by * in (inset a) are due to impurities of Co_3O_4 precursor. Both P3 and P3' samples are the sample as listed in Table 2.

inset b) and that of P3' (Fig. 4 inset a), the monoclinical splitting of P3 104, 015, 107 and 018 peaks can be clearly observed in P3'. A Rietveld refinement has also been carried out in space group R3m (No. 160) for P3 and the results were given in Table 2.

Additional steps, like the one at x=0.50, as shown in Fig. 8b, in P3' single phase region indicates the existence of certain Sodium ion vacancy ordering in P3', which is not presented in this study. The 003 peaks of O3 phase have a fixed position

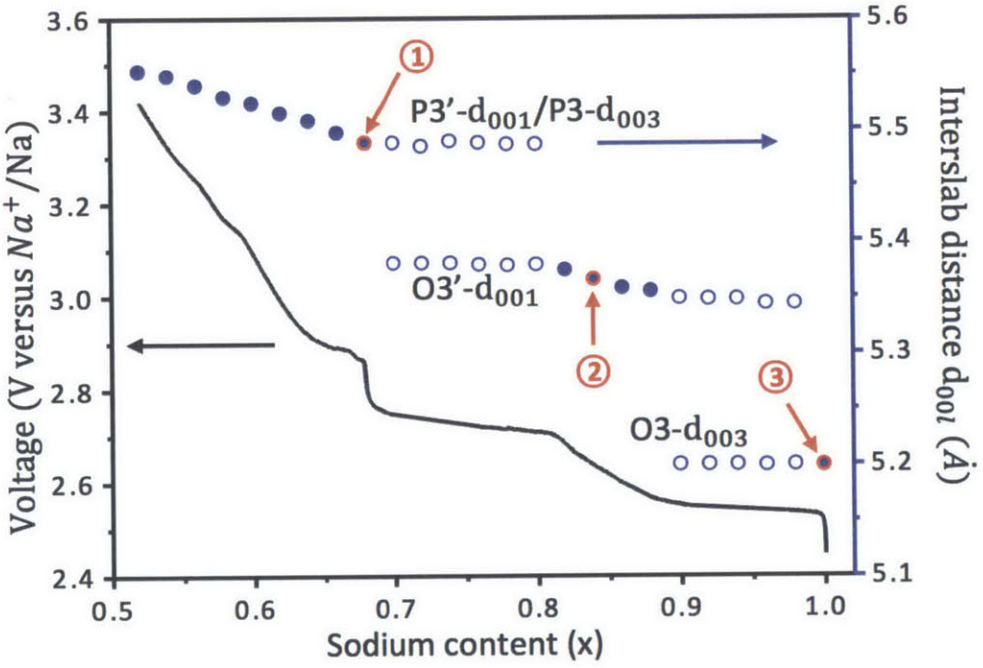

Figure 5 | Calculation of the interslab distance d_{00l} of O3, O3' and P3/P3' as a function of sodium content x. The sodium content in three-layer Na_xCoO_2 influences the phase transitions as well as the interslab distance in each phase, which could be calculated according to the $00l$ peak positions. The d_{00l} remains constant in biphasic domains (open circles) while increases continuously in single-phase regions (filled blue circles) during sodium deintercalation. The data points in red circles labeled with 1, 2 and 3 are P3'-$Na_{0.67}CoO_2$, O3'-$Na_{0.83}CoO_2$ and O3-$Na_{1.00}CoO_2$ respectively, whose interslab distances are most comparable to that of those P3', O3' and O3 samples synthesized by solid-state reaction.

(corresponding to a constant interslab distance $d_{003} = 5.200\ A$), in either single O3 phase region or two phase region with O3'. The 001 peak of O3' phase have fixed positions in two phase regions with O3 or with P3', but an obvious shift of the 001 peak towards low angle (corresponding to an increase in d_{001} interslab distance) is observed in the single phase domain upon further charging. The behavior of the 003 peaks of P3' phase is similar to that of O3', the peak position is fixed in the two-phase region with O3' but shifts towards low angle (corresponding to an increase in d_{003} interslab distance) in single-phase region during charging. This result is generally consistent with previous reports[2,11]. The electrochemical charge curve of O3-$Na_{1.00}CoO_2$ battery exhibits a slightly higher voltage in the *in situ* XRD experiment (Fig. 3 right side) than in the normal charge tests using Swaglok cells (Fig. 8b). For example, the corresponding voltage of the P3 phase at x=0.56 is 3.22v and 3.15v respectively using the two different methods. This known issue is associated with the more significant polarization in the cells designed for *in situ* XRD due to contact problems.

3.3 Structure Comparison of Single Phase

3.3.1 O3 Type

In this study, a total number of four samples of O3 phase, with $\phi_{Na:Co}$=0.92, 0.96, 1.00, 1.05 respectively were obtained at 450°C without forming other layered compound. A Rietveld refinement has been done to give lattice parameters of these samples as a function of $\phi_{Na:Co}$, as shown in Fig. 6a. All samples have the same interslab distance ($d_{003} = c_{tri}/3 = 5.200 \pm 0.003\ \dot{A}$) and the same a_{tri} lattice constant

($a_{tri} = 2.889 \pm 0.001\ \dot{A}$) within margin of error. In addition, based on a careful examination of the XRD patterns of these four samples, only the sample with $\phi_{Na:Co} = 1.05$ does not exhibit any impurity peak, while an increasing amount of Co_3O_4 has been observed as $\phi_{Na:Co}$ decrease from 1.00 to 0.92 in the other three samples. Fig. 7a shows the increase of Co_3O_4 311 peak intensity.

3.3.2 O3' Type

Another five samples of O3' phase, with $\phi_{Na:Co}$=0.68, 0.76, 0.84, 0.92, 1.00 were synthesized at 500°C, 515°C, 550°C, 650°C, 650°C respectively without containing any other layer compounds. A Rietveld refinement has been carried out to give lattice parameters of these samples as a function of $\phi_{Na:Co}$, as shown in Fig. 6b. Similar to the case of O3 phase, all O3' samples have the same or very close interslab distance, $d_{001} = c_{mon} \times \cos(\beta - \frac{\pi}{2}) = 5.363 \pm 0.003\ \dot{A}$, and the same a_{mon} lattice constant, $a_{mon} = 4.896 \pm 0.002\ \dot{A}$, within margin of error. An examination of the XRD patterns of these five samples in detail shows that the samples with $\phi_{Na:Co} > 0.84$ does not exhibit any Co_3O_4 impurity peak, while an increasing amount of Co_3O_4 has been observed as $\phi_{Na:Co}$ decrease from 0.84 to 0.68 in the other three samples. Fig. 7b shows the increase of Co_3O_4 311 peak.

3.3.3 P3' Type

As can be found in Fig. 2, six samples fall into P3' single phase region without contamination of other layered compounds, with $\phi_{Na:Co}$=0.60, 0.68, 0.72, 0.74, 0.60 and 0.68 and T=550°C, 550°C, 550°C, 550°C, 500°C and 535°C respectively. The lattice parameters of these samples as a function of $\phi_{Na:\square o}$, were also given based on

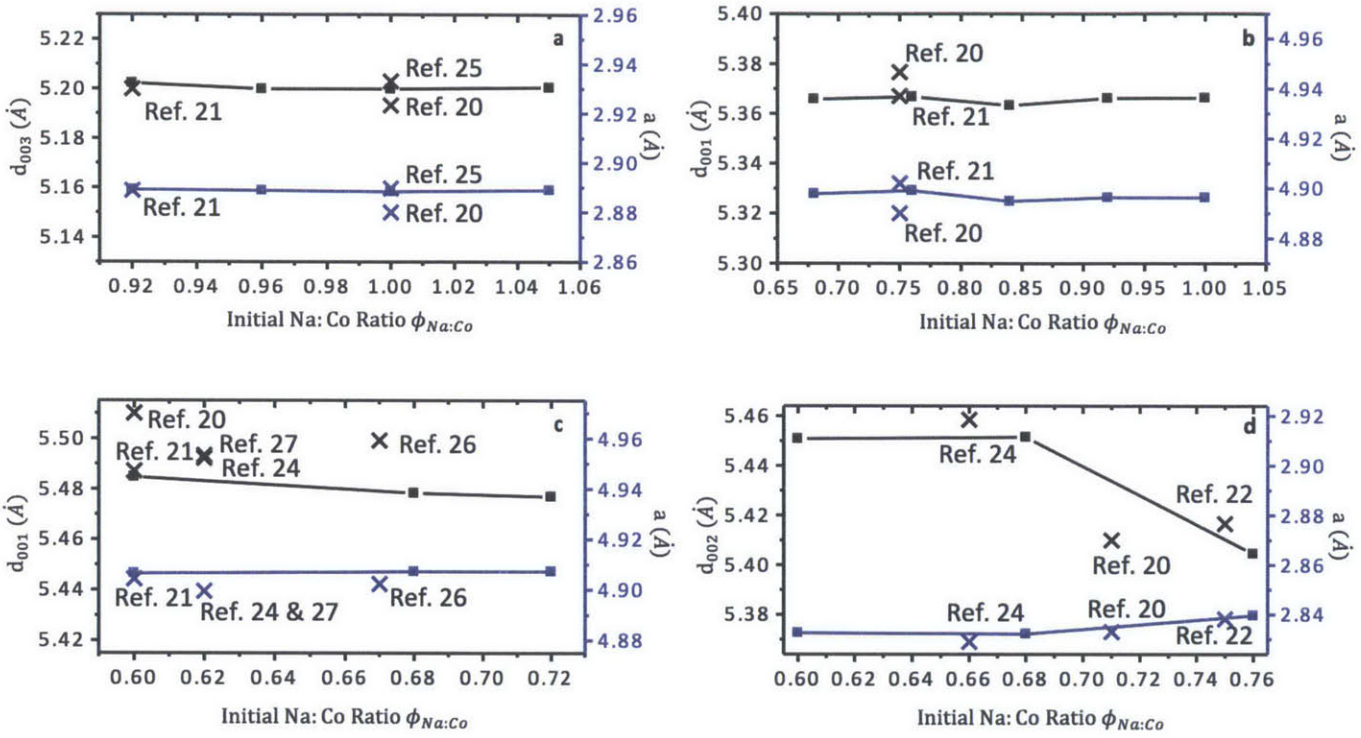

Figure 6 | Variations of interslab distance d_{001} (in black) and horizontal lattice constant a (in blue) as a function of initial Na:Co ratio for O3 (a), O3' (b), P3' (c) and P2 (d) samples in nominal single-phase regions. Four of O3 samples, three of P3' samples and three of P2 samples in (a), (c) and (d) were obtained at 450°C, 550°C and 750°C respectively. While five of O3' samples in (b) were synthesized at 500°C, 515°C, 550°C, 650°C and 650°C individually from left to right. The invariability of d_{001} and a found in O3, O3' and P3' is the sign that these samples have almost the same x regardless of different $\phi_{Na:Co}$. Only P2 samples exhibit a variable x as a function of $\phi_{Na:Co}$. The comparison of our results (filled square) with previous experimental studies (crosses) shows a decently good consistency of O3, O3' and P2 phases, while our P3' samples exhibit slightly smaller d_{001} in all compositions, which indicates our P3' samples may have more Na in the layered compound than nominal values. The result of Ref. 4 in (d) is a calculated average value based on their original data and Ref. 8 in (a) is a single crystal O3 sample.

Rietveld refinements, as shown in Fig. 6c. All P3' samples were also found to have very close interslab distance, $d_{001} = c_{mon} \times \cos(\beta - \frac{\pi}{2}) = 5.480 \pm 0.003\ \dot{A}$, and almost the same a_{mon} lattice constant, $a_{mon} = 2.824 \pm 0.002\ \dot{A}$, within margin of error. The XRD patterns of these five samples show the existence of certain amount of Co_3O_4 in all five of P3' samples. Fig. 7c shows the presence of Co_3O_4 311 peak.

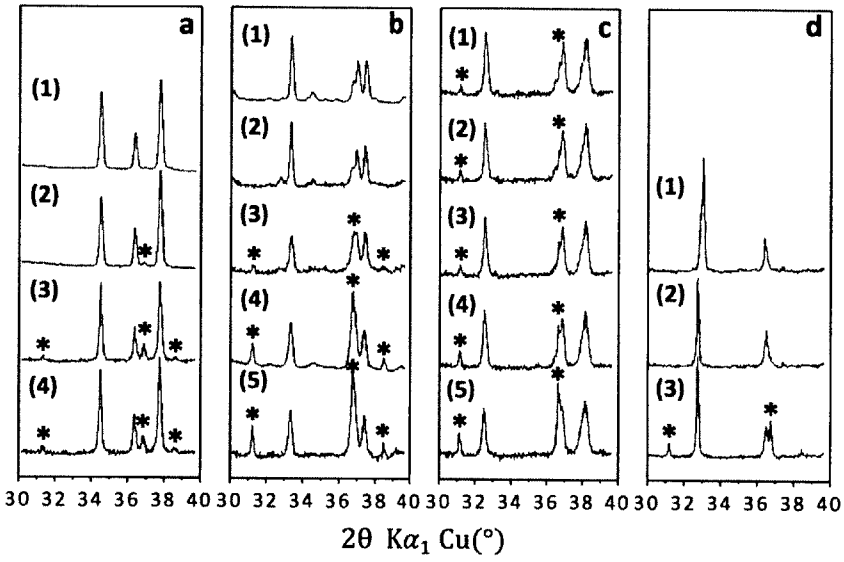

Figure 7 | A comparison of the XRD patterns of O3 (a), O3' (b), P3' (c) and P2 (d) samples in nominal single-phase regions from 30° to 40°. Four of O3 samples in (a) were obtained at 450°C with $\phi_{Na:Co}$=1.05 (1), 1.00 (2), 0.96 (3) and 0.92 (4). Five of O3' samples in (b) have different synthesis conditions: T=650°C and $\phi_{Na:Co}$=1.00 (1), T=650°C and $\phi_{Na:Co}$=0.92 (2), T=550°C and $\phi_{Na:Co}$=0.84 (3) and T=515°C and $\phi_{Na:Co}$=0.76 (4), T=500°C and $\phi_{Na:Co}$=0.68 (5). Five of P3' samples in (c) also have different synthesis conditions: T=550°C and $\phi_{Na:Co}$=0.72 (1), T=550°C and $\phi_{Na:Co}$=0.68 (2), T=535°C and $\phi_{Na:Co}$=0.68 (3) and T=550°C and $\phi_{Na:Co}$=0.60 (4), T=500°C and $\phi_{Na:Co}$=0.60. The synthesis temperature of three of P2 samples in (d) is 750°C with $\phi_{Na:Co}$=0.76 (1), 0.68 (2), 0.60 (3). Peaks marked by * are Co_3O_4 impurities.

3.3.4 P2 Type

Only three samples synthesized at 750°C in the selected range of interest turn out to be P2 phase. No other layer structure were found when $\phi_{Na:Co}$=0.60, 0.68, 0.76. Unlike the other three phases, a Rietveld refinement of their XRD patterns indicates that the sample with $\phi_{Na:Co}$=0.60 and the sample with $\phi_{Na:Co}$=0.68 have almost the same lattice parameters ($d_{002} = c_{hex}/2 = 5.451 \pm 0.001\ \dot{A}, a_{hex} = 2.831 \pm 0.001\ \dot{A}$) while compared to the other two, the sample with $\phi_{Na:Co}$=0.76 has smaller d_{002} but larger a_{hex} ($d_{002} = c_{hex}/2 = 5.403\ \dot{A}, a_{hex} = 2.840\ \dot{A}$). The XRD patterns confirmed the purity of the samples with $\phi_{Na:Co}$=0.68 and 0.76, while the other one, with $\phi_{Na:Co}$=0.60, contains small amount of Co_3O_4 impurity, as shown in Fig. 7d.

CHAPTER 4

DISCUSSIONS

4.1 Electrochemical Behaviors of Na_xCoO_2

4.1.1 Phase Transformation of the three layer type

As reported previously[11-16] in various systems, an O3-O3'-P3/P3' transition in the three layer structure is typical during electrochemical deintercalation of Na ions from these layered compounds. Our *in situ* study clearly unveils a phase evolution of the three-layer type Na_xCoO_2 during sodium deintercalation. Starting with a pure O3 phase, the intensity of reflection corresponding to the O3 phase 003 plane at 2θ=7.795° decreases immediately upon charging with an increase in the intensity of the peak at 2θ=7.580°, indicating the transformation of the O3 phase into O3' phase in the range of $0.88<x<1$. This O3-O3' transformation happens through a monoclinic distortion resulting from a gliding of CoO_2 layers coupled with Na deficiency. Upon further Na ion deintercalation, the intensity of O3'-001 peak decreases accompanied by an increase in the intensity of P3'-001 peak at 2θ=7.382°, indicating another phase transformation in the range of $0.67<x<0.81$. During the O3'-P3' transition, Na ions become prismatically instead of octahedrally coordinated by oxygen; this is because the prismatic environment for Na ions is more thermodynamically favored when CoO_2 layers become less negatively charged. On further deintercalation of Na ions in the range of $0.54<x<0.56$ and $0.57<x<0.59$, the successive biphasic transitions of P3'-P3 and P3-P3' could be identified based on the observation of a combination the P3'-201 and P3'-$\bar{1}$12 peak followed by the monoclinic splitting of P3-015 peak, as shown in Fig. 3 top left inset. The reason for this transition is still unknown, but we notice previous study has proved that the

P3'-P3 transition in the Na_xCoO_2 system could be attributed to the breaking of certain Na vacancy ordering upon heating[27]. In addition, the three layer structure to P2 or reverse transformation has never been observed during electrochemical deintercalation of Na in our experiment, this is because such transformation requires not only CoO_2 layer shifts but also a $\pi/3$ rotation of all CoO_6 octahedra, meaning Co-O bond breaking is required during such transformation[11].

4.1.2 Visualization of Monoclinical Distortion

In order to visualize the monoclinical distortion from O3 to O3' and from P3 to P3', a coordinate system transformation has been done for both O3' and P3' so that they have comparable lattice parameters with O3 and P3 (results given in Table 3). Despite the change of a, b and c, O3 phase transforms into O3' mainly through an increase of β angle from 90.00° to 94.81°, which can be roughly considered as a glide of CoO_2 layers in the $\bar{1}00$ direction. The x-z plane (parallel to the paper surface) of O3 and O3' structure were shown in Fig. 1a inset and Fig. 1b inset respectively to visualize the resulting distortion effect caused by a β angle change. A distorted (or tilted) structure of O3' can be easily identified when compared to its parent structure O3. Similarly, P3' phase has a slightly smaller β and γ angle than the undistorted P3 structure. If we look at the x-z plane of the P3' phase, as shown in Fig. 1c inset, a very small amount of CoO_2 layer gliding in the 100 direction can be identified. The dashed line in Fig. 1c inset is perpendicular to the x axis in the x-z plane thus can be used as a reference to observe the relatively insignificant monoclinical distortion of the P3' phase.

Table 3. The transformation of the coordinate systems of monoclinically distorted P3' and O3' into those of undistorted P3 and O3. The P3', P3, O3' and O3 samples are the same as those listed in Table 2.

O3' in its original coordinate system	O3' in the coordinate system the same as O3	O3
$a = 4.8912$ $b = 2.8681$ $c = 5.7937$ $\alpha = 90.000°$ $\beta = 111.843°$ $\gamma = 90.000°$	$a = 2.8350$ $b = 2.8681$ $c = 16.2100$ $\alpha = 90.000°$ $\beta = 94.810°$ $\gamma = 120.387°$	$a = 2.8883$ $b = 2.8883$ $c = 15.6019$ $\alpha = 90.000°$ $\beta = 90.000°$ $\gamma = 120.000°$
P3' in its original coordinate system	**P3' in the coordinate system the same as P3**	**P3**
$a = 4.9126$ $b = 2.8270$ $c = 5.7087$ $\alpha = 90.000°$ $\beta = 106.064°$ $\gamma = 90.000°$	$a = 2.8340$ $b = 2.8270$ $c = 16.4584$ $\alpha = 90.000°$ $\beta = 89.477°$ $\gamma = 119.919°$	$a = 2.8192$ $b = 2.8192$ $c = 16.5880$ $\alpha = 90.000°$ $\beta = 90.000°$ $\gamma = 120.000°$

4.1.3 Thermodynamics

In the *in situ* XRD experiment, the identified phase variations in the XRD patterns match very well with the features found on the charge curve. Biphasic domains correspond well to the plateaus on charge curve while steeper steps characterize those singe-phase regions. This result is consistent with our understanding about the thermodynamics of two-phase transition, during which the composition of each phase (thus the interslab distance) stays constant while the proportion of each phase changes when the overall composition increase or decrease. The voltage plateau, therefore, is a direct result of the fixed compositions of the two relevant phases. The increase of the interslab distance and of the voltage in single-phase regions can be attributed to the solid solution behavior of the material.

4.2 Determination of Na Content in each sample

4.2.1 O3 Type

Unlike previous reports, our study shows that O3 phase can only form O3-$Na_{1.00}CoO_2$ by either solid-state reaction or electrochemical deintercalation/intercalation. Pure O3 phase can only be synthesized using solid-state reaction when $\phi_{Na:Co}$ is equal to or slightly larger than 1.00 (considering a possible small amount of Na loss during the synthesis process); when $0.92<\phi_{Na:Co}<1.00$, O3-$Na_{1.00}CoO_2$ coexists with Co_3O_4 impurity, as shown in Fig. 7a. The observation of the increasing intensity of Co_3O_4 311 peak in XRD profiles with decreasing $\phi_{Na:Co}$ values and the fact that all four samples of O3 have exactly the same lattice parameters (Fig. 6a) are two strong evidences to support this conclusion. This assumption is also confirmed by electrochemical deintercalation and *in situ* XRD experiment; O3' phase emerges immediately upon the start of charge process of O3 cathode. Even in the biphasic domain of O3+O3' during electrochemical deintercalation, the O3-d_{003} values stays constant, indicating that O3 also stays stoichiometrical in the biphasic region.

4.2.2 O3' Type

In contract to earlier studies on O3'-Na_xCoO_2, our experiment and observation indicate O3' phase can only form O3'-$Na_{0.83}CoO_2$ by solid-state reaction even if we set $\phi_{Na:Co}$ in a large range from 0.68 to 1.00. We found that for all O3' samples, they have $d_{001}\approx5.365\dot{A}$ as shown in Fig. 6b; and the corresponding sodium composition,

x=0.83, can be easily read from the O3' d_{001}-x relation calculated based on *in situ* XRD experiment. The data points marked by number 2 in Fig. 5 is O3'-$Na_{0.83}CoO_2$ that has the closest interslab distance with that of those synthesized O3' samples. The conclusion that O3' can only form $Na_{0.83}CoO_2$ is also consistent with the observation of increasing amount of Co_3O_4 impurity as $\phi_{Na:Co}$ decreases from 0.84 to

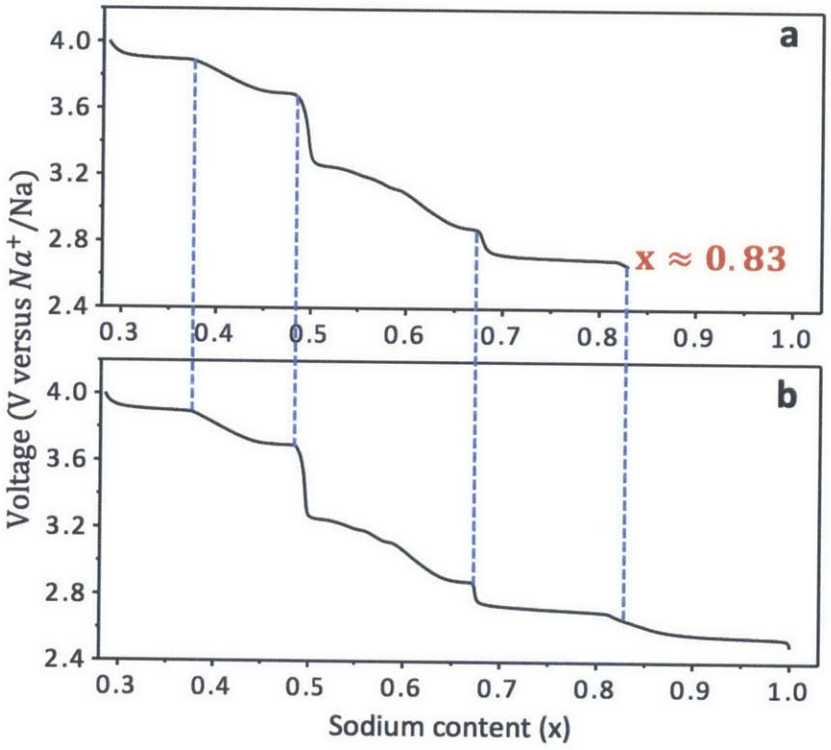

Figure 8 | A comparison between the galvanostatic charge curves of O3'-Na_xCoO_2 with T=650℃, $\phi_{Na:Co}$=1.00 (a) and that of O3-$Na_{1.00}CoO_2$ with T=450℃, $\phi_{Na:Co}$=1.05 (b) batteries. Both batteries were charged to 4.0 volts at the rate of C/20 (12 mA g^{-1}) under room temperature. The charge curve of O3 cathode exhibits exactly the same features as Fig. 3 had shown In the 0.52<x<1.00 range, while more steps and plateaus were found when x>0.52, which may correspond to superstructures and ordering of Na ions in P3' phase. The charge curve of O3' cathode highly matches that of O3 if the two curves were aligned according to the features found at the same voltage (blue dashed lines). By shifting the O3' curve and making it overlap with that of the O3, the initial composition in O3'-Na_xCoO_2 x≈0.83 could be read directly.

0.68, while no additional Co_3O_4 were found in samples with $\phi_{Na:Co}$ >0.84. This indicates when $\phi_{Na:Co}$<0.83, excessive Co exists in the form of Co_3O_4 that coexists with O3'-$Na_{0.83}CoO_2$; and when $\phi_{Na:Co}$>0.83, excess Na may have already evaporated during sintering. Another comparison between the charge curve of an O3' battery with nominal composition $\phi_{Na:Co}$ =1.00 and that of an O3 cathode with composition $Na_{1.00}CoO_2$ was made, as shown in Fig. 8. Two charge curves have been aligned according to the steps and features they share in common at the same voltage so that the two curves can overlap well. An initial composition of x=0.83 can be easily read based on this comparison, which again confirms that O3' forms $Na_{0.83}CoO_2$. O3' phase with other compositions x, from 0.81 to 0.88, corresponding to 5.375 $\dot{A}$ >d_{001}>5.350 $\dot{A}$, can be obtained by electrochemical deintercalation of Na. We notice that 0.83≈ 5/6, which indicates the possible reason for O3'-$Na_{5/6}CoO_2$ being stable is the formation of some superstructure or vacancy ordering of Na, which was first mentioned in 1973[20], and observed by TEM later[21].

4.2.3 P3' Type

Similar to the case of O3 phase and O3' phase, samples that form P3' phase also have almost the same lattice parameters, as shown in Fig. 6c. Again, this is a sign that all samples of P3' have similar Na composition in the layered structure even the nominal value ranges from 0.60 to 0.72. Unlike other three phases, however, all P3' samples contain small amount of Co_3O_4 impurity, shown in Fig. 7c, under the experimental conditions in this work. A comparison has been made between the P3' d_{001}-x relation calculated according to the *in situ* XRD experiment

and the interslab distances of those obtained by solid-state reaction. It is found that P3' d_{001}=5.480 $\dot{A}$ corresponds to x=0.67 (number 1 in Fig. 5), near the boundary between P3' monophasic region and P3'+O3' biphasic domain. This indicates P3' can only form $Na_{0.67}CoO_2$ by solid-state reaction. On the other hand, P3'-Na_xCoO_2 with x<0.67, can be obtained by electrochemical Na deintercalation.

4.2.4 P2 Type

Among the four phases of Na_xCoO_2 synthesized by solid-state reaction in this work, P2 phase is the only phase that stays pure in a relatively larger range of Na content, that is 2/3<x<3/4. An obvious d_{002} spacing increase is observed when $\phi_{Na:Co}$ decreases from 0.76 to 0.68, as shown in Fig. 6d; this is consistent with an actual Na content decrease in the layered structure in these samples. The conclusion that P2-$Na_{0.68}CoO_2$ and P2-$Na_{0.76}CoO_2$ samples are pure and their nominal Na content are the same as the actual Na content in the layered structure, is not only supported by the purity of their XRD patterns, as shown in Fig. 7d, but can also be verified by a comparison of P2 d_{002}-x relation with that of the In situ XRD experiment of P2 reported previously[4]. When 0.60<x<0.68, however, P2-$Na_{0.68}CoO_2$ forms and it coexists with excessive Co which exists in the form of Co_3O_4. This can be easily confirmed by the existence of Co_3O_4 311 peak in the XRD pattern of P2 with $\phi_{Na:Co}$ =0.60 (Fig. 7d). And the invariability of P2 d_{002} spacing, when 0.60<x<0.68, indicates the P2 phase we obtained in this range have exactly the same Na content, which is around 0.68 or 2/3.

CHAPTER 5

CONCLUSIONS AND THESIS STATEMENT

5.1 Synthesis Diagram of Na_xCoO_2

In this work, a complete and uniform synthesis diagram of Na_xCoO_2 is determined for the first time; a total number of 41 samples of Na_xCoO_2 with $0.60<\phi_{Na:Co}<1.05$ were successfully synthesized between 450°C and 750°C, revealing four monophasic domains and four biphasic regions. All four phases of Na_xCoO_2 that can be synthesized by solid-state reaction reported earlier, α (also O3), α' (also O3' or O1), β (also P3' or P1) and γ (also P2), were obtained in this work. And the sodium content x in Na_xCoO_2 for all single-phase samples synthesized were determined by comparing their interslab distance d_{00l} to the d_{00l}-x relation obtained by an *in situ* XRD experiment. It is found that O3, O3' and P3' samples synthesized by solid-state reaction can only form with single stoichiometry under the applied synthesis conditions in this study; they are O3-$Na_{1.00}CoO_2$, O3'-$Na_{0.83}CoO_2$ and P3'-$Na_{0.67}CoO_2$ respectively. The P2 phase, however, can form in a relatively larger sodium content range, from P2-$Na_{0.68}CoO_2$ to P2-$Na_{0.76}CoO_2$ instead.

A direct visualization of the monoclinical distortion from O3 to O3' and from P3 to P3' is realized by transforming the coordinate systems of O3' and P3' phase into those of O3 and P3 so that they have comparable lattice constants. It is found that for both P3' and O3' phase, such monoclinical distortion could be attributed mainly to a β angle change, which could be easily observed by looking at the x-z plane of the structures.

5.2 Electrochemistry of Na_xCoO_2

An *in situ* XRD experiment was carried out during the electrochemical deintercalation of Na ions from O3-$Na_{1.00}CoO_2$ battery to unveil the phase variations in the three layer structures of Na_xCoO_2. Successive phase transformations of O3-O3'-P3'-P3-P3' have been observed and monophasic domains of O3, O3', P3' and P3 were identified in our experiment based on a correlation between the *in situ* XRD patterns and the electrochemistry of the three layer type Na_xCoO_2. The d_{00l}-x relations for O3, O3' and P3/P3' phase were calculated according to the *in situ* XRD profiles. It is also found for the first time that under room temperature P3 phase Na_xCoO_2 is observed in a very narrow composition range near $x \approx 0.56$.

REFERENCES

1. Delmas, C., Fouassier, C. & Hagenmuller, P. Structural classification and properties of the layered oxides. *Phys. B+C* **99,** 81–85 (1980).

2. Yoshida, H., Yabuuchi, N. & Komaba, S. NaFe0.5Co0.5O2 as high energy and power positive electrode for Na-ion batteries. *Electrochem. commun.* **34,** 60–63 (2013).

3. Yabuuchi, N. *et al.* P2-type Nax[Fe1/2Mn1/2]O2 made from earth-abundant elements for rechargeable Na batteries. *Nat. Mater.* **11,** 1–6 (2012).

4. Berthelot, R., Carlier, D. & Delmas, C. Electrochemical investigation of the P2-Na(x)CoO(2) phase diagram. *Nat. Mater.* **10,** 74–80 (2010).

5. Shu, G. & Chou, F. Sodium-ion diffusion and ordering in single-crystal P2-NaxCoO2. *Phys. Rev. B* **78,** 3–6 (2008).

6. Zandbergen, H., Foo, M., Xu, Q., Kumar, V. & Cava, R. Sodium ion ordering in NaxCoO2: Electron diffraction study. *Phys. Rev. B* **70,** 1–8 (2004).

7. Roger, M. *et al.* Patterning of sodium ions and the control of electrons in sodium cobaltate. *Nature* **445,** 631–4 (2007).

8. Meng, Y. S., Hinuma, Y. & Ceder, G. An investigation of the sodium patterning in Na(x)CoO(2) (0.5 < or = x < or = 1) by density functional theory methods. *J. Chem. Phys.* **128,** 104708 (2008).

9. Lee, D. H., Xu, J. & Meng, Y. S. An advanced cathode for Na-ion batteries with high rate and excellent structural stability. *Phys. Chem. Chem. Phys.* **15,** 3304–12 (2013).

10. Lu, Z. & Dahn, J. R. In situ X-ray diffraction study of P2-Na2/3[Ni1/3Mn2/3]O2. *J. Electrochem. Soc.* **148,** A1225–A1229 (2001).

11. Delmas, C., Braconnier, J., Fouassier, C. & Hagenmuller, P. Electrochemical intercalation of sodium in NaxCoO2 bronzes. *Solid State Ionics* **3-4,** 165–169 (1981).

12. Sathiya, M., Hemalatha, K., Ramesha, K., Tarascon, J.-M. & Prakash, A. S. Synthesis, Structure, and Electrochemical Properties of the Layered Sodium Insertion Cathode Material: NaNi1/3Mn1/3Co1/3O2. *Chem. Mater.* **24,** 1846–1853 (2012).

13. Saadoune, I., Maazaz, A., Menetrier, M. & Delmas, C. On the NaxNi0.6Co0.4O2 system: physical and electrochemical studies. *J. Solid State Chem.* **122,** 111–117 (1996).

14. Komaba, S. *et al.* Study on the Reversible Electrode Reaction of Na1-xNi0.5Mn0.5O2 for a Rechargeable Sodium-Ion Battery. *Inorg. Chem.* **51,** 6211–6220 (2012).

15. Zhou, Y.-N. *et al.* Phase transition behavior of NaCrO2 during sodium extraction studied by synchrotron-based X-ray diffraction and absorption spectroscopy. *J. Mater. Chem. A* **1,** 11130–11134 (2013).

16. Takeda, Y. *et al.* Sodium Deintercalation from Sodium Iron Oxide. *Mater. Res.* **29,** 659–666 (1994).

17. Shacklette, L. W., Jow, T. R. & Townsend, L. Rechargeable Electrodes from Sodium Cobalt Bronzes. **135,** 2669–2674 (1988).

18. Terasaki, I., Sasago, Y. & Uchinokura, K. Large thermoelectric power in NaCo2O4 single crystals. *Phys. Rev. B* **56,** 685–687 (1997).

19. Takada, K. *et al.* Superconductivity in two-dimensional CoO2 layers. *Nature* **422,** 53–55 (2003).

20. Fouassier, C., Matejka, G., Reau, J. & Hagenmuller, P. Sur de Nouveaux Bronzes Oxygenes de Formule NaxCoO2 (x<1). Le Systeme Cobalt-Oxygene-Sodium. **6,** 532–537 (1973).

21. Viciu, L. *et al.* Crystal structure and elementary properties of NaxCoO2 (x=0.32, 0.51, 0.6, 0.75, and 0.92) in the three-layer NaCoO2 family. *Phys. Rev. B* **73,** 174104 (2006).

22. Huang, Q. *et al.* Coupling between electronic and structural degrees of freedom in the triangular lattice conductor NaxCoO2. *Phys. Rev. B* **70,** 184110 (2004).

23. Huang, Q. *et al.* Low temperature phase transitions and crystal structure of Na0.5CoO2. *J. Phys. Condens. Matter* **16,** 5803–5814 (2004).

24. Carlier, D. *et al.* Sodium ion mobility in Na(x)CoO2 ($0.6 < x < 0.75$) cobaltites studied by 23Na MAS NMR. *Inorg. Chem.* **48,** 7018–7025 (2009).

25. Takahashi, Y., Gotoh, Y. & Akimoto, J. Single-crystal growth, crystal and electronic structure of NaCoO2. *J. Solid State Chem.* **172,** 22–26 (2003).

26. Ono, Y. *et al.* Crystal Structure, Electric and Magnetic Properties of Layered Cobaltite β-NaxCoO2. *J. Solid State Chem.* **166,** 177–181 (2002).

27. Blangero, M. *et al.* High-temperature phase transition in the three-layered sodium cobaltite P'3-NaxCoO2(x~0.62). *Phys. Rev. B* **77,** 184116 (2008).